Erschienen in: Advanced Functional Materials ; 29 (2019), 19. - 1808331
https://doi.org/10.1002/adfm.201808331

Multifunctional Block Copolymers for Simultaneous Solubilization of Poorly Water-Soluble Cholesterol and Hydroxyapatite Crystals

*Philipp Keckeis, Eliška Drabinová, Cristina Ruiz-Agudo, Jonathan Avaro, Lisa Glatt, Miloš Sedlák, and Helmut Cölfen**

The solubilization of targeted compounds represents key criteria in the sophisticated field of medical chemistry but also in technical applications like scale removal. Especially, the simultaneous dissolution of two chemically different compounds remains challenging. Herein, macromolecular solubilizers are introduced for the simultaneous dissolution and encapsulation of poorly water-soluble cholesterol and hydroxyapatite. The peptide-based, amphiphilic block copolymers possess physicochemically disparate segments combined in one polymer chain as binding sites for hydrophobic as well as ionic materials. Small polymer libraries are synthesized and screened for structure–property relationships. Complementary analytical techniques suggest polymeric self-assembly into spherical adaptive nanoparticles with the fundamental ability to passively absorb significant amounts of hydrophobic cholesterol up to 33 wt%. Furthermore, the additional incorporation of acidic domains enables the simultaneous dissolution of hydrophobic compounds and mineral phases such as hydroxyapatite. Ultimately, those nontoxic block copolymers can be used to solubilize and absorb other lipophilic and ionic compounds such as Sudan III dye and calcium ions. Such multifunctional nanomaterials have a wide range of direct application for simultaneous dissolution or delivery of hydrophobic molecules and cations resp. minerals for instance in the field of atherosclerosis.

1. Introduction

The uptake of poorly water-soluble pharmaceutical compounds plays a fundamental role in the field of drug delivery, whereby specific block copolymers mediate the solubilization of commonly hydrophobic materials. Block copolymers offer the beneficial potential to form various self-organized morphologies,[1–3] like, e.g., polymer scaffolds for the incorporation of guest molecules. Therefore, such macromolecules find various nanotechnological applications in drug delivery, gene delivery, staining, etc.[4–7] For instance, double hydrophilic block copolymers (DHBC) and amphiphilic block copolymers possess the inherent structural properties of both segments combined in one polymer chain. This includes the joint of one noninteracting water-soluble block and a second solvophilic resp. solvophobic block with pendant specific functionalities to promote interaction with charged or hydrophobic targets, respectively.[8] Therefore, enhancing the solubility of guest substances and the protection from enzymatic opsonization present collaborated key characteristics that qualify such copolymers as promising nanocarriers.[9] Most of the established systems include the solubilization and encapsulation of only one pharmaceutical compound in nano-objects. Beyond that, the idea of a binary cargo is of great interest regarding the enhanced efficiencies.[10–12] Lv et al. demonstrated that the codelivery of paclitaxel and doxorubicin embedded in steroidal-functionalized PEG polypeptide nanovehicles facilitates synergistic anticancer effects.[13] However, one of the key quantities governing the simultaneous incorporation of physicochemically disparate substances is characterized by the ability to solubilize hardly soluble materials. Therefore, solubilizing agents need to mediate dissolution by overcoming lattice energies, which are generally high for mineral phases, e.g., for hydroxyapatite (HAP),[14] or by enhancing the water solubility of poorly soluble hydrophobic substances due to the hydrophobic effect.[15] Theories of lipophilic drug solubilization are described elsewhere.[16,17] In the center of this conundrum, two almost water-insoluble materials, HAP (solubility product 2.91×10^{-58} M^9 at 25 °C)[18] and cholesterol (solubility at 30 °C 1.8 µg mL^{-1} = 0.07×10^{-6} M),[19] were exposed to designed polymers. One relevant research field deals with the solubilization of cholesterol in the course of direct dissolving atherosclerotic plaques, which trigger

P. Keckeis, Dr. C. Ruiz-Agudo, Dr. J. Avaro, L. Glatt, Prof. H. Cölfen
Physical Chemistry
University of Konstanz
Universitätsstraße 10, Box 710, 78467 Konstanz, Germany
E-mail: helmut.coelfen@uni-konstanz.de
Dr. E. Drabinová, Prof. M. Sedlák
Institute of Organic Chemistry and Technology,
Faculty of Chemical Technology
University of Pardubice
Studentská 573, 532 10 Pardubice, Czech Republic

atherosclerosis—the cause of death among 40% of the western hemisphere.[20] A promising strategy includes the application of cyclodextrin (β-CD) to improve the cholesterol solubilization.[21] For instance, methylated β-cyclodextrin solution (10×10^{-3} M) was found to solubilize cholesterol (1.1×10^{-3} M) corresponding to 3.2 wt% cholesterol loading at 25 °C and 4.4 wt% at 37 °C, respectively, via the formation of 1:2 cholesterol/CD chelate complex.[22] Based on this capability, β-CD derivates are applied in the field of atherosclerosis in order to mediate cholesterol efflux from macrophages[23,24] and to reverse atherosclerosis regression as detected by in vivo experiments.[25] Further drug delivery approaches with the potential to renew atherosclerotic therapies that mediate cholesterol efflux and plaque regression are described elsewhere.[26–30] They all have the cholesterol dissolution in common.

Block copolymers are also interesting as mineral scale inhibitors. The precipitation of slightly soluble inorganic salts in water-based industrial processes (e.g., chemical manufacturing, cement operations, food processing, oil industry, and medical instruments) represents a common phenomenon that causes production losses and major costs. For instance, the incrustation of calcium minerals (carbonates, sulfates, phosphates, and oxalates) leads to hardly soluble mineral deposits clogging pipes and equipment and thus reducing the efficiency of technological processes.[31–33] The formation of calcium phosphate scale is of special interest since the inorganic phase is one of the most frequently occurring materials in biologically mineralized systems. The dynamic equilibrium process between crystallization and redissolution was studied by Nancollas and Wu.[34] As a sequel, Peytcheva and Antonietti applied polymer additives to investigate the solubilization of calcium phosphate (brushite) and demonstrated the partial dissolution of the {010} crystal surface by polyaspartate (M_n = 18 kg mol^{-1}) at pH = 8.1.[35] With the aim of inhibiting scale formation, polyelectrolytes have been for decades the most used strategy.[36] In this context, designed multifunctional block copolymers present a wide range of novel compounds that could be employed to prevent mineral scaling.

Here, a wide range of physicochemical properties of peptide-based, multifunctional block copolymers (**Figure 1**) are introduced in this study including the ability to simultaneously solubilize physicochemically disparate substances, such as hydrophobic compounds and mineral hydroxyapatite. We detail the synthesis and structural characterization of the polymeric nanoassociates and their capacity to absorb both hydrophobic and ionic compounds. The intended design of these macromolecules to target specific absorption content qualify them as critical solubilization agents, e.g., as carriers for drug delivery and in the field of atherosclerosis since atherosclerotic plaques are composed of hydrophobic cholesterol crystals and mineral hydroxyapatite scale.

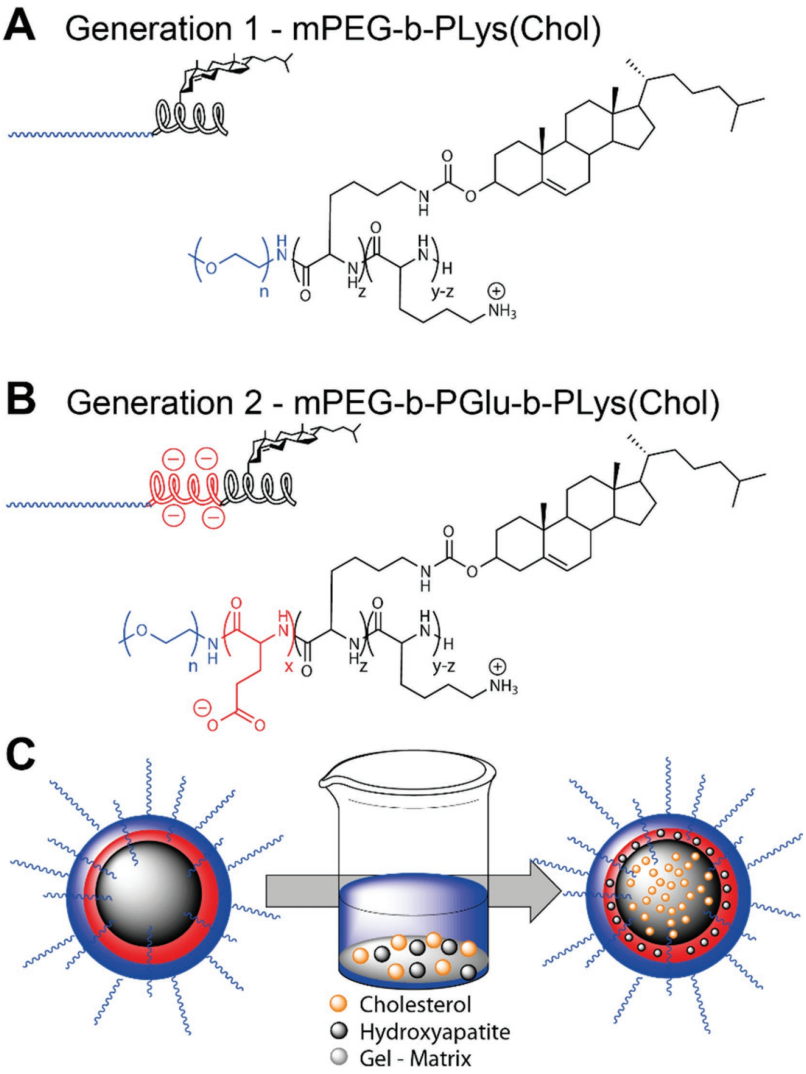

Figure 1. Chemical structures of amphiphilic generation 1 diblock copolymer mPEG-*b*-PLys(Chol) A) and generation 2 triblock copolymer mPEG-*b*-PGlu-*b*-PLys(Chol) B), and schematic self-assembly and capability to solubilize hydrophobes and hydroxyapatite C).

2. Results and Discussion

2.1. Amphiphilic G1 Polymers

2.1.1. Synthesis

The first generation of polymers (**G1**) was synthesized (Figure S1, Supporting Information) including amphiphilic diblock copolymers with a hydrophilic polyethylene glycol (PEG) block and a hydrophobic segment of cholesteryl-grafted polylysine. Different copolymers were synthesized via living ring-opening polymerization of carboxybenzyl-lysine *N*-carboxyanhydride initiated by a PEG amine macroinitiator.[37] The polymer backbones constitute narrow molecular weight distributions and the protecting groups were cleaved with trifluoroacetic acid. Post-polymerization modification with cholesteryl chloroformate results in amphiphilic block copolymers with hydrophobic contents ranging from 8 to 29 mol% (**Table 1**). The detailed

Table 1. Synthesized amphiphilic **G1** copolymers, particle sizes and cholesterol absorption.

Entry	Copolymers **G1**[a]	PDi[b] $M_w M_n^{-1}$	Hydrophobic content[c] [mol%]	Size of the particles[d] D_H [nm]	Size of the Chol-loaded particles[d] D_H [nm]	Trapped Chol molecules per unimer[c]	Absorbed Chol content[c] [wt%]
G1–1	$mPEG_{113}$-*b*-$PLys_{7.3}(Chol)_{2.5}$	1.28	19	20	92	2.7	13
G1–2	$mPEG_{113}$-*b*-$PLys_{4.2}(Chol)_{2.4}$	1.29	21	18	47	3.6	18
G1–3	$bisPEG_{226}$-*b*-$PLys_{9.0}(Chol)_{4.1}$	1.19	29	21	88	15.8	33
G1–4	$mPEG_{113}$-$(Chol)_{1.0}$	1.15	8	13	62	5.7	29

[a]The subscripts of $mPEG_{113}$-*b*-$PLys_{7.3}(Chol)_{2.5}$ indicate the stoichiometric polymer composition of on average 113 CH_2–CH_2–O and 7.3 lysine repetition units, and 2.5 cholesteryl molecules, as estimated by proton NMR analysis; [b]GPC analysis in THF against PS standard; [c]^{1}H-NMR compositional analysis; [d]DLS: number-weighted diameter.

synthetic procedures and all characterization data are provided in Figures S2–S15 in the Supporting Information.

2.1.2. Structural Analysis

Polymer dispersions (0.5 mg mL^{-1}) were prepared by ordinary solution method and structurally characterized (**Figure 2**; Figures S16–S24, Supporting Information). Fluorescence measurements of pyrene solubility reveal critical micelle concentration (cmc) values of $10^{-6.5}$ M in the typical range for amphiphilic block copolymers.[38] Zeta-potential measurements suggest slightly positive charges (e.g., ζ-potential +1.06 mV) due to positively charged residual free amine moieties at physiological pH. Dynamic light scattering (DLS) reveals nanometer-sized hydrodynamic diameters between 13 and 21 nm (Table 1). The DLS sizes include the number weighted diameters, which represent the intrinsic distribution of the particle population. In contrast, the intensity-weighted size distribution is based on the measured scattering intensity depending upon R_H^6. Thus, larger species exert a much greater influence on the scattering intensity than smaller particles until the detection limit of the smaller objects.[39] This might mislead to overproportional presence of the bigger species, which heavily skews the particle population toward larger particle sizes. For a complete overview, all DLS data (intensity-weighted and number-weighted size distributions) are given in Sections S6.2 and S7.2.1 in the Supporting Information. In addition, analytical ultracentrifugation analysis shows the presence of one species with low sedimentation coefficients (Figure 2B). Combining this structural data of the amphiphilic copolymers gives rise to the conclusion of self-assembled, stable nanoassociates.

2.1.3. Cholesterol Absorption

The potential to absorb cholesterol inside the polymer particles was investigated in detail using standardized experiments (Figure 1). The amount of absorbed cholesterol was quantified by proton NMR compositional analysis (Figures S25–S29, Supporting Information) ranging from 2.7 up to 15.8 cholesterol molecules per unimer, or respectively 13 to 33 wt% (Table 1). It is worth to mention that the backbone PEG–$PLys_7$ itself does not absorb cholesterol (Figure S25, Supporting Information). The highest amount of absorbed cholesterol was observed in the case of the bis-terminal copolymer **G1–3**, which is interesting considering the bis-PEG chain representing a BAB-type triblock copolymer. Analytical ultracentrifugation (AUC) and DLS both show a significant increase of the sedimentation coefficients resp. particle sizes up to ≈50–90 nm (Table 1) in all model solutions of prepared **G1** copolymers after cholesterol absorption (Figure 2A,B, dashed curve; Figures S16–S23, Supporting Information). The polydispersity essentially remains unchanged after cholesterol addition.

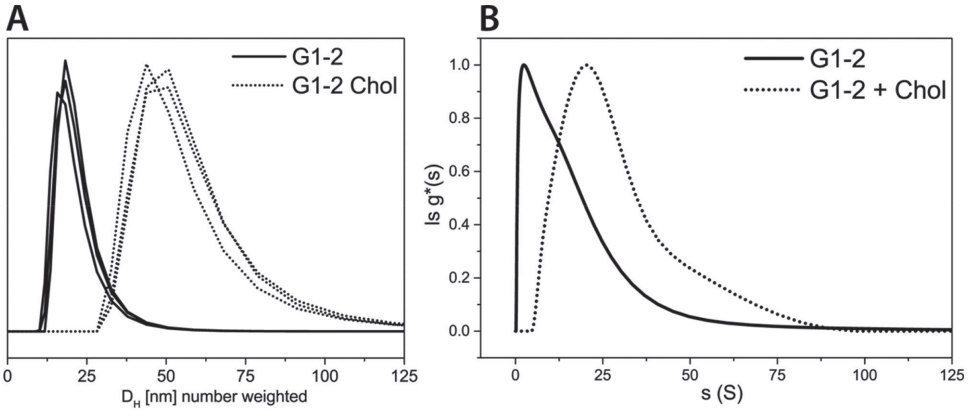

Figure 2. Structural analysis of cholesterol absorbed **G1–2** polymer. Dynamic light scattering measurement A) and normalized, nondiffusion-corrected sedimentation coefficient distribution from AUC measurement of native **G1–2** dispersion and cholesterol-loaded **G1–2** dispersion B).

In summary, synthesized **G1** copolymers passively dissolve remarkable amounts of poorly water-soluble cholesterol (up to 33 wt%) and bind the molecules in stable nanoassociates. Nevertheless, the AB-type, amphiphilic block copolymers dissolve and absorb remarkable amounts of free cholesterol, especially **G1–4**, which can be synthesized rapidly. Since common drug delivery systems usually load from 10 to 40 wt% of pharmaceutical compounds and required accurate preparation methods, these macromolecular solubilizers have promising chaperone and carrier/delivery properties for hydrophobic molecules.[17]

2.2. Multifunctional G2 Polymers

2.2.1. Synthesis

The second generation of multifunctional triblock copolymers **G2** was synthesized (Figure S1, Supporting Information) including an incorporated polyglutamic acid domain as negatively charged binding site to achieve electrostatic interactions with calcium ions besides cholesterol uptake. Details of the polymer syntheses and the characterization data are provided in Figures S30–S43 in the Supporting Information. mPEG amine was applied as macroinitiator for ring-opening polymerization of γ-benzyl glutamic acid-*N*-carboxyanhydride prior to the addition of carboxybenzyl-lysine *N*-carboxyanhydride. The PEG-peptide backbone with a narrow molecular weight distribution of = 1.13 (Figure S32, Supporting Information) was simultaneously deprotected with trifluoroacetic acid and hydrobromic acid. NMR and MALDI TOF spectral analysis demonstrated the quantitative deprotection and the presence of the polyelectrolyte backbone after deprotection (Figures S33–S34, Supporting Information). A library of **G2** copolymers with increasing hydrophobic content was synthesized by cholesterol grafting (**Table 2**) and purified via dialysis.

2.2.2. Structural Analysis

The aqueous polymeric dispersions (0.5 mg mL^{-1}) were prepared by dissolution techniques and structurally characterized (Figures S45–S65, Supporting Information). The increase of the hydrophobic content induces the reduction of the aqueous solubility until the fully modified polymer **G2–5** is almost insoluble (Figure S45, Supporting Information). The pyrene solubility depending on the concentration of the polymer dispersions was measured by fluorescence probe technique revealing a decrease of the cmc values from 13.7 to 3.1 mg L^{-1} with increasing hydrophobic content. Such values are in accordance with the expected order of magnitude of 10^{-6} molar for amphiphilic block copolymers.[38] Zeta-potential measurements exhibit an increase of negative charges with increasing cholesteryl content due to the reduction of positively charged amine groups. Light scattering measurements suggest particle sizes in the nanometer range (20–60 nm) increasing with the hydrophobic content. As discussed above, the DLS sizes include the number weighted size distribution. Apparently, the fine-tuning of the polarities by variation of the cholesteryl content substantially affects the morphologies. In conclusion, the **G2** copolymers present adaptive self-assembly of negatively charged, nanosized particles.

2.2.3. Hydrophobic Absorption

The properties of the polymers to solubilize hydrophobic molecules were studied in basic test systems (Figure 1), applying Sudan III dye and cholesterol as representatives for extremely lipophilic substances. After the separation of nonbound hydrophobes, the total amount of dissolved targets was quantified by UV–vis measurements. **G2–3** and **G2–4** absorbed respectively 5.9 and 3.5 wt% Sudan III (Figure S66, Supporting Information). Cholesterol absorption experiments demonstrate the capacity of those polymers to solubilize 6.3 wt% (**G2–3**) and 1.2 wt% (**G2–4**) cholesterol within the polymeric particles, determined by UV–vis measurements applying the Liebermann–Burchard reagent (Figures S67–S72, Supporting Information).[40] The blank polymer backbone mPEG–$PGlu_{12}$–$PLys_{11}$ does not absorb cholesterol at all (Figure S68, Supporting Information). The fine-tuning of the **G2** polymer polarities reveals the most favorable composition for hydrophobic solubilization of the **G2–3** derivate, whereas lower or too high cholesteryl contents reduce the cholesterol absorption. The solubilization experiments first demonstrate that the polymers overcome the lattice energy of a solid cholesterol crystal and dissolve significant parts of it. Second, the capacity to dissolve hydrophobic materials is independent of the molecular structure of the incorporated guest molecule since loading values are in excellent agreement for both hydrophobic molecules. Additionally, it is noteworthy, opposite to common solvent exchange methods

Table 2. Synthesized multifunctional **G2** copolymers, structural analysis, and cholesterol absorption.

Entry	Copolymers G2[a)]	Hydrophobic content[b)] [mol%]	CMC[c)] [mg L^{-1}]	Zeta-potential [mV]	Size of the native particles[d)] D_H [nm]	Size of the Chol-loaded particles[d)] D_H [nm]	Trapped Chol molecules per unimer[e)]	Absorbed Chol content[e)] [wt%]
G2–1	$mPEG_{113}$-*b*-$PGlu_{12}$-*b*-$PLys_{11}(Chol)_{0.5}$	3	13.7	−8.1	24	26	0.2	1.0 (0.1)
G2–2	$mPEG_{113}$-*b*-$PGlu_{12}$-*b*-$PLys_{11}(Chol)_{1.5}$	10	13.3	−13.0	16	42	0.6	2.6 (0.8)
G2–3	$mPEG_{113}$-*b*-$PGlu_{12}$-*b*-$PLys_{11}(Chol)_{4.0}$	23	7.6	−34.3	26	122	1.7	6.3 (1.4)
G2–4	$mPEG_{113}$-*b*-$PGlu_{12}$-*b*-$PLys_{11}(Chol)_{7.5}$	37	3.2	−38.0	38	209	0.4	1.2 (0.3)
G2–5	$mPEG_{113}$-*b*-$PGlu_{12}$-*b*-$PLys_{11}(Chol)_{11}$	48	3.1	−27.3	59	n.d.	n.d.	n.d.

[a)]The subscripts of $mPEG_{113}$-*b*-$PGlu_{12}$-*b*-$PLys_{11}(Chol)_{0.5}$ indicate the stoichiometric polymer composition of on average 113 CH_2–CH_2–O, 12 glutamic acid and 11 lysine repetition units, and 0.5 cholesteryl molecules, as estimated by proton NMR analysis; [b)]^{1}H-NMR compositional analysis; [c)]CMC fluorescence measurement; [d)]DLS: number-weighted diameter; [e)]UV–vis measurement applying the Liebermann–Burchard reagent in triplicates (standard deviation).[40]

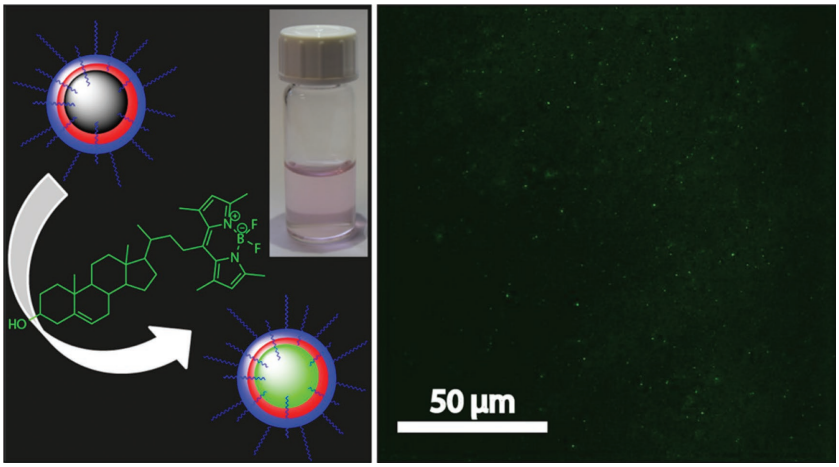

Figure 3. Confocal fluorescence microscopy analysis of **G2–2** polymer dispersion after solubilization of fluorescent BODIPY-cholesterol. The inset shows the polymeric dispersion after filtration of nonbound fluorescent dye via syringe filter (200 nm).

to achieve high drug-loading capacities, that the hydrophobic absorption is passive here. Furthermore, thermal analysis suggests a homogenous dissolution of cholesterol molecules within the hydrophobic particle core[41] whereas microphase separation is unlikely (Figure S73, Supporting Information).[42]

Fluorescent BODIPY-cholesterol (23-(dipyrromethen-eboron difluoride)-24-norcholesterol)[43] was used to visualize the encapsulated cholesterol within **G2–2** polymer conjugates (**Figure 3**; Figures S74–S76, Supporting Information). Fluorescence microscopy reveals the presence of small fluorescent dots after the separation of nonbound BODIPY-cholesterol, which were absent in reference experiments performed without polymer or with nonfluorescent cholesterol. This unambiguously demonstrates the capacity of the **G2–2** polymer to absorb cholesterol.

2.2.4. Structural Analysis after Cholesterol Loading

According to DLS measurements, cholesterol absorption leads to increased particle sizes for **G2** polymers (Table 2). CryoTEM analysis of the native **G2–2** polymer dispersion (**Figure 4**A; Figure S52, Supporting Information) indicates nanosized particles around 40 nm in diameter, still present after cholesterol absorption (Figure 4B) and further worm-like nano-objects probably disorganized assemblies. Nevertheless, the micellar stability is given, as soon as the cmc is exceeded. This is demonstrated by concentration-dependent DLS investigation of **G2–2** (Figure S53, Supporting Information) where the size distribution was found concentration independent, as well as in time-resolved, DLS monitored titration experiments revealing constant size distribution (**Figure 5**C). AUC sedimentation data (Figure 4C) reveal two small but significantly different sedimentation coefficients s = 0.06 and 0.78 S suggesting the presence of two native polymer species. Morphological stability is proven by the presence of these species after cholesterol absorption, although cholesterol absorption leads

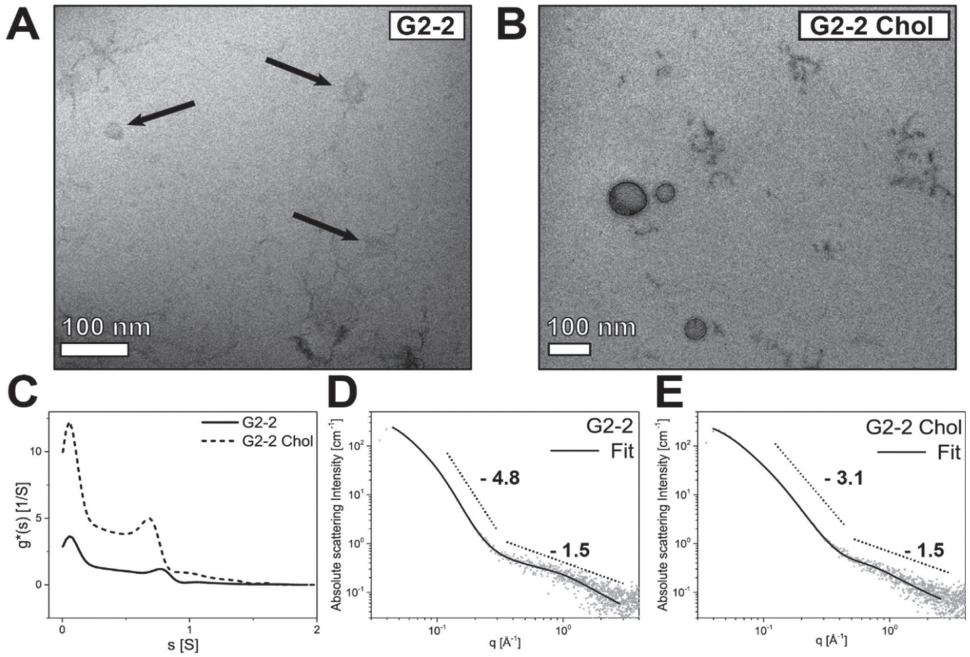

Figure 4. CryoTEM, AUC, and SAXS analysis of cholesterol absorption by **G2–2** polymer. CryoTEM microscopic images of a native **G2–2** dispersion A) and of after cholesterol absorption B). Scale bars: 100 nm. C) Nondiffusion corrected sedimentation coefficient distribution AUC measurement of native **G2–2** dispersion and cholesterol-loaded **G2–2** dispersion. Synchrotron-derived SAXS analysis of native **G2–2** polymer dispersion D) and of cholesterol-loaded **G2–2** polymer dispersion E).

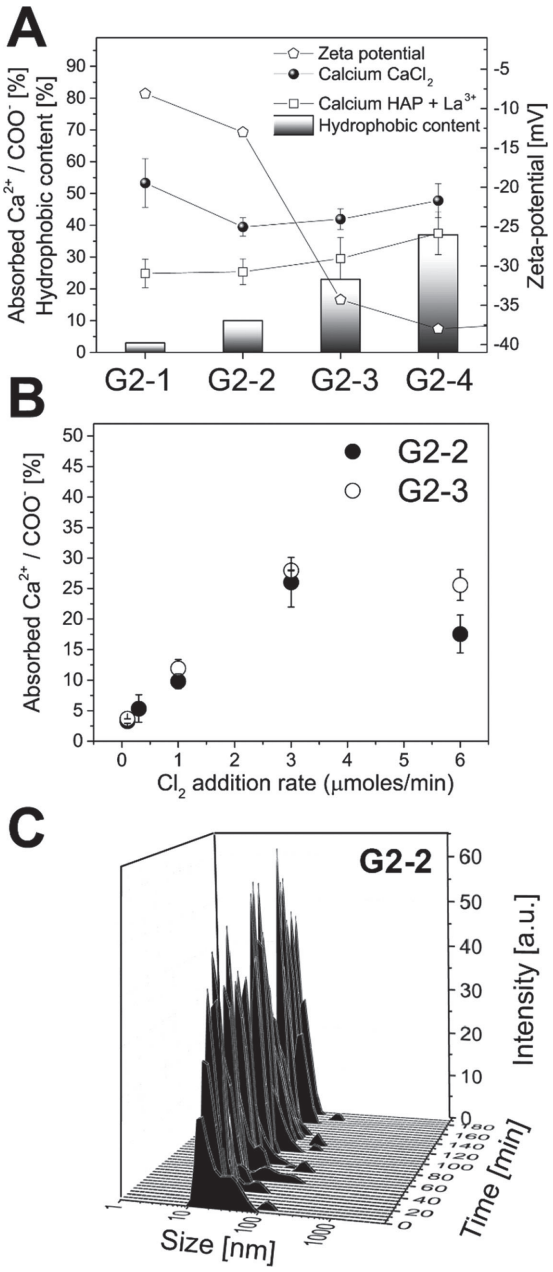

Figure 5. A) Interaction between **G2** polymers and calcium ions. Absolute quantities of absorbed calcium ions by **G2** polymers measured with atomic absorption spectroscopy (triplicates) from supersaturated $CaCl_2$-solution (black circles) and hydroxyapatite (white squares) in the presence of lanthanum chloride (10.000 ppm). B) Addition-dependent calcium absorption of **G2–2** (black circles) and **G2–3** (white circles) polymer dispersions applying potentiometric titration. C) Time-dependent DLS monitoring of **G2–2** titration with 100×10^{-3} M $CaCl_2$ solution with addition rate of 0.03 mL min^{-1}.

to an increase of the detected concentration and the maxima slightly decrease.

Synchrotron-based SAXS analysis for the native **G2–2** dispersion (Figure 4D,E and for other **G2** polymers see Figures S62–S65 and Table S1 in the Supporting Information) reveals two structural levels for native and cholesterol absorbed **G2–2** dispersion characterized by distinct power law. Porod slope values (Q) of ≈1.5 translate to mass fractal structures for homogeneous sample, e.g., branched-like morphologies or spherical object of different size for polydisperse sample. Values of $Q \approx 4$ represent spherical objects, including polymeric micelles and negative deviation from the Porod law, which are usually characteristics of spherical objects possessing a diffuse interface.[44] Consequently, SAXS data suggest single polymer chains representing the first structural level with mass fractal structure and radius of gyration (r_{G2}) of 3.9 nm, which constitute the building block for larger spherical objects possessing a radius of gyration $r_{G1} > 34.0$ nm ($r_{G1} >$ beamline size limitation), e.g., polymeric micelles representing the second structural level. Cholesterol absorption does not affect the morphology of single polymer chains ($r_{G2} = 5.3$ nm), whereas the second structural level shows slight morphological changes ($Q_1 = 3.1$), potentially spherical objects with rough surfaces or clustered networks with $r_{G1} > 34.0$ nm. Combination of structural analytical methods converges to the conclusion that the **G2–2** polymer self-assembles into nanometer-sized, spherical micelles while substantially maintaining their stature after cholesterol absorption. It is noteworthy that the most cholesterol absorbing **G2–3** polymer forms spherical micelles after cholesterol encapsulation ($Q = 4.4$; $r_G = 10.6$ nm).

The negatively charged glutamic acid domain obviously interferes with the hydrophobic core, leading to hampered cholesterol solubilization compared to **G1** polymers. However, the incorporation of two completely physicochemically disparate features in one unimer requires the compromise between reduced cholesterol absorption and the ability for dual dissolution of different substances.

2.2.5. Calcium Absorption

The mineral solubilization capacity of the designed polymers was tested in calcium rich system. Such ions usually well soluble by the formation of hexahydrated constructs can form at the same time hardly soluble minerals with high lattice energies. Therefore, the interactions between **G2** polymers and calcium ions were investigated with respect to the dissolution and binding capacities. Figure 5A shows the relationship between different **G2** copolymer architectures and the affinity to absorb calcium ions, either from $CaCl_2$ solution or from hardly soluble hydroxyapatite. Calcium uptake was quantified by atomic absorption spectroscopy (AAS). First, calcium absorption capacity was determined by the excessive supersaturation of the polymeric dispersions with calcium ions (1000 μmol) and isolation from nonbound ions by centrifugation. AAS reveals absorbed calcium ion contents of 2.1–3.1 wt% corresponding to 0.39–0.53 calcium ions per carboxylic acid group (Figure S77, Supporting Information). Those binding values are in good agreement with those found for absorbed calcium by polymeric hydrogels containing acetic acid moieties (0.39–0.45 Ca^{2+}/COO^-).[45] On the other hand, **G2** polymers were investigated with respect to uptake of calcium ions, bound in hardly soluble hydroxyapatite crystals (Figure S78, Supporting Information). Hence, the polymer dispersions were isolated from excess solid hydroxyapatite after stirring overnight and the absorbed

calcium content was determined by AAS measurement in the presence of lanthanum(III) chloride to mask the intervening phosphates (Figure 5A, white squares).[46] Ca^{2+}/COO^- values from 0.25 to 0.38 were quantified for the **G2** polymers, which increase with higher hydrophobic cholesteryl contents. Considering the architectural changes of the **G2** polymers, two inverse trends are obvious. On the one hand, the blank backbone mPEG-*b*-$PGlu_{12}$-*b*-$PLys_{11}$ is supposed to self-assemble upon the formation of polyionic complexes[47] by oppositely charged electrostatic pair interactions between amine and glutamic acid moieties (Figure S79, Supporting Information), whereas, on the other hand, in the case of **G2–4** mPEG-*b*-$PGlu_{12}$-*b*-$PLys_{11}(Chol)_{7.5}$, intermolecular binding is mainly induced by hydrophobic interactions. Here, cholesteryl grafting basically reduces the presence of amine moieties and provides glutamic acid groups for calcium binding. This correlates with the negative surface charges (−8.1 to −38.0 mV) of the polymeric associates and increased the quantity of absorbed calcium ions bound in hydroxyapatite. Finally, the experiments demonstrate the ability of the multifunctional polymer to overcome the lattice energy of hydroxyapatite and to dissolve calcium ions from the mineral.

With the aim of getting better insights into calcium affinity of the **G2** polymers, calcium absorption was further investigated by potentiometric titration. This is a well-established technique to understand and quantify binding processes such as absorption by polyanionic polymers.[32] Experiments were carried out by the stepwise addition of $CaCl_2$ to **G2–2** and **G2–3** polymer dispersions at physiological pH (7.4). Ca^{2+} potential was monitored via an ion selective electrode and the activity of free Ca^{2+} in solution inferred from a calibration curve realized by adding free calcium ions to Milli-Q water under a nitrogen shower. Free Ca^{2+} profiles (discussed in detail in Figures S80–S83 in the Supporting Information) suggest that binding capacities of the **G2–2** and **G2–3** polymers via ion exchange mechanism are sensitively dependent on the $CaCl_2$ addition rate. It was found that the amount of Ca^{2+} ions per COO^- group ranged from 0.06 to 0.25 with increasing Ca^{2+} addition rate from 0.01 to 3 µmol calcium ions per min (Figure 5B). Those calcium binding values are similar to the ones found for well-known systems of polyaspartic acid with the capability to absorb 0.16–0.29 calcium ions per carboxylic acid, depending on the molecular weight.[32] Titration experiments with still faster Ca^{2+} addition rates (6 µmol min^{-1}) suffer from ionic strength effects and slow-moving equilibrium reactions decreasing Ca^{2+} binding values. Additionally, in situ DLS measurements during titration experiments do not display any significant changes of the particle size upon calcium binding by **G2–2** polymer (Figure 5C).

2.2.6. Simultaneous Sudan III, Cholesterol, and Calcium Absorption

In order to set more realistic scenario, the environmental conditions were changed to assess the polymers capacity to solubilize Sudan III dye, cholesterol and calcium ions used as representatives for lipophilic and ionic components. First, the total amount of the polymer-absorbed dye and calcium was quantified via UV–vis and AAS measurements. **G2–3** polymer absorbs 2.4 wt% Sudan III and 0.38 Ca^{2+}/COO^- and **G2–4** polymer 2.9 wt% Sudan III and 0.44 Ca^{2+}/COO^-, respectively (Figure S84, Supporting Information). Compared to Sudan III uptake in absence of calcium ions (**G2–3**: 5.9 wt% and **G2–4**: 3.5 wt%; Figure S66, Supporting Information), the hydrophobic encapsulation is slightly reduced by the presence of calcium ions, presumable due to repulsive interactions.

Second, the environmental conditions have been tightened up by replacing the media with an ionic blood-mimicking solution and furthermore, by covering the targeted compounds in a gel matrix of kappa-carrageenan. **G2–2** polymer was dispersed in a blood-mimicking medium (exempt of calcium ions),[48] in the presence of solid cholesterol and hydroxyapatite (Figures S85 and S86, Supporting Information). **G2–2** polymer was found to simultaneously absorb 4 wt% cholesterol and 1 wt% calcium (0.17 Ca^{2+}/COO^-). The increased quantity of absorbed cholesterol (2.6 wt% in Milli-Q) presumably results from the cationic shielding of glutamic acid functions reducing repulsive interactions between hydrophobic cholesterol molecules and negatively charged carboxylate groups. The calcium absorption from HAP is also reduced possibly by other cationic species in the blood-mimicking media competing with calcium ions. Finally, artificial gel models of kappa-carrageenan, which are pervaded with cholesterol and mineral hydroxyapatite, should impede polymer-induced solubilization process (Figures S87 and S88, Supporting Information). Here, **G2–2** was found to extract 0.1 wt% cholesterol and 0.18 wt% calcium (0.03 Ca^{2+}/COO^-), which is low compared with other experiments but still underscores the dissolution process even in complex environments.

2.3. Cytotoxicity Assays

Further investigations of the interaction of the designed polymers with a biological system were performed. The native **G1–2** and **G2–2** polymer conjugates were additionally examined in ex vivo cell viability and cell death assays using the renal proximal tubule epithelial cell line RPTEC/TERT1 and the Alamar Blue (or resazurin) and lactate dehydrogenase (LDH) leakage assays, respectively (Figure S89, Supporting Information).[49] Living cells metabolize nonfluorescent resazurin to fluorescent-active resorufin by autoreduction while dying cells, on the other hand, rupture and release their content including enzymes like LDH into the cell culture supernatant. Consequently, cell viability was quantified via fluorescent measurement and cell death can be assessed by quantification of extracellular LDH activity. Resorufin fluorescence data obtained for **G1–2** and **G2–2** showed no loss of viability for the tested concentrations. In fact, some treatments resulted in values larger than 100% (**Figure 6**). The data suggest that at the given concentrations both compounds do not impair cellular viability and none of the compounds caused cell death as determined by LDH leakage. Therefore, any acute substantial interference between the multifunctional triblock copolymers with essential functions of RPTEC/TERT1 cells is unlikely. Clarification whether the observed stimulation of resazurin reduction by RPTEC/TERT1 cells in presence of **G1–2** and **G2–2** is a specific effect would need further investigation using alternative cell viability assays.

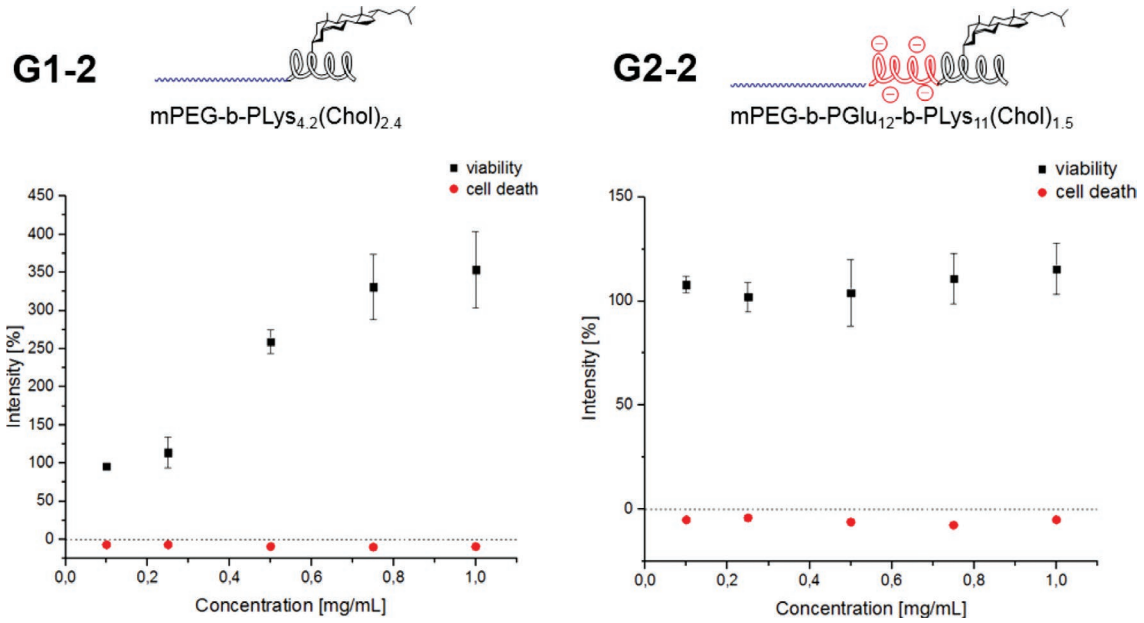

Figure 6. Cytotoxicity assays of **G1–2** and **G2–2** dispersions using renal proximal tubule epithelial cell line RPTEC/TERT1 for 72 h. Viability assay based on resorufin as fluorogenic indicator (black squares). Lactate dehydrogenase leakage assay (red circles) in order to asses cell deaths in % of the change toward the control experiments. The data points represent the mean of three technical triplicates and are normalized to 100% untreated cells.

3. Conclusion

In summary, we have presented multifunctional block copolymers as solubilizers for hardly soluble substances with physicochemical disparate properties, such as hydrophobic cholesterol or Sudan III molecules and calcium ions dissolved from hydroxyapatite. We could demonstrate the self-organization of amphiphilic generation 1 polymers, based on PEG–polylysine with covalently attached cholesteryl moieties, into nanoparticles with the inherent capacity to dissolve significant amounts of free cholesterol, up to 33 wt%. We have further developed a second generation of multifunctional triblock copolymers with an additional incorporated glutamic acid domain as binding sites for calcium ions besides cholesterol absorption. Complementary analytical techniques suggest self-assembly of the polymer into nanosized spherical micelles simultaneously incorporating up to 4 wt% cholesterol and 1 wt% calcium ions, dissolved from mineral hydroxyapatite. Based on the remarkable capacity to dissolve and encapsulate different target substances, those polymers have high potential for applications as nanocarriers for drug delivery, or used for antiscaling actions, both for technological and biological scales. Furthermore, the **G2** block copolymers constitute macromolecular surfactants, which potentially solubilize hazardous deposits in the body namely atherosclerotic plaques that are composed of hardly soluble cholesterol and hydroxyapatite. Therefore, we currently investigate the intracellular cholesterol uptake in our laboratories.

4. Experimental Section

Polymer Synthesis: In brief, α-amino-ω-methoxy-poly(ethylene glycol) (M_n = 5000 g mol^{-1}) was used as macroinitiator to induce ring-opening polymerization of γ-benzyl glutamic acid-*N*-carboxyanhydride (BzGlu-NCA) at 25 °C in dimethyl formamide for 4 days. The evolved CO_2 was removed under reduced pressure. After complete conversion, carboxybenzyl-lysine *N*-carboxyanhydride (ZLys-NCA) was added and stirred for further 4 days. A white powder was obtained after precipitation in diethylether. Side chain protection groups of mPEG-*b*-PBzGlu-*b*-PZLys were cleaved with trifluoroacetic acid and hydrobromic acid and the PEG peptides were purified by dialysis. Finally, the amine functions were modified with cholesteryl chloroformate and potassium carbonate in a water acetone (1:1) mixture. The crude product was purified by exhaustive dialysis and trituration with diethylether (Supporting Information).

Characterization of NPs: Polymer dispersions were obtained by dissolution of solid polymer in Milli-Q water (0.5 mg mL^{-1}) and stirring overnight, prior to filtration (syringe filter 200 nm, Micropur, PVDF). The hydrodynamic diameter of NPs, shape, surface charge and CMC were determined in aqueous dispersions by dynamic light scattering, small-angle X-ray scattering and zeta-potential measurements (Zetasizer Nano ZSP, Malvern), and by fluorescence measurements via pyrene solubility (FluoTime300, PicoQuant). Analytical ultracentrifugation (Beckman-Coulter XL-I) was applied to measure the size distribution of the particles. (Supporting Information).

Quantification of Absorbed Cholesterol: Solid cholesterol was added to the polymer dispersions and stirred overnight prior to the filtration of nonbound cholesterol. The cholesterol-loaded particles were isolated by lyophilization and triturated with diethylether in order to extract the absorbed cholesterol. The amount of entrapped cholesterol was quantified via ^{1}H-NMR spectral analysis for G1 polymers (Figures S25–S29, Supporting Information) and by UV–vis spectroscopy applying the Liebermann–Burchard reagent for G2 polymers (Figures S68–S72, Supporting Information), respectively.

Quantification of Absorbed Calcium from $CaCl_2$ Solution: Excess $CaCl_2$ was added to the polymer dispersions. After stirring overnight, the dispersion was centrifuged at 9000 rpm for 60 min, prior to redispersion of the solid sediment in water and repeated centrifugation. The calcium absorbed polymer dispersion was analyzed by atomic absorption spectroscopy in order to quantify the calcium content (Figure S77, Supporting Information).

Quantification of Absorbed Calcium by $CaCl_2$ Titration: Potentiometric titration experiments were carried out using a commercially available titration setup manufactured by Methrom equipped with calcium selective electrode and pH electrode. Calcium addition to polymer

dispersions was varied to asses bound calcium by **G2–2** and **G2–3** (Figures S80–S83, Supporting Information).

Quantification of Absorbed Calcium from Hydroxyapatite: Hydroxyapatite was added to the polymer dispersions. After stirring overnight, the dispersion was filtrated to remove solid hydroxyapatite. The calcium absorbed polymer dispersion was analyzed by atomic absorption spectroscopy in order to quantify the calcium content (Figure S78, Supporting Information). Due to the phosphate interference, each sample contained 10.000 ppm $LaCl_3$ in order to mask the phosphates.

Blood-Mimicking Media with Cholesterol: The polymer was dispersed in a medium composed of $NaHCO_3$, $MgCl_2$, NaH_2PO_4, KCl, and NaCl in Milli-Q in the presence of cholesterol. The cholesterol and calcium absorbed polymer was obtained by lyophilization after purification via filtration and centrifugation. The absorbed cholesterol was extracted by trituration with diethylether and quantified by UV–vis spectroscopy applying the Liebermann–Burchard reagent. The absorbed calcium was quantified by AAS (Figures S85 and S86, Supporting Information).

Artificial Atherosclerotic Plaques: Kappa-carrageenan was intermixed with cholesterol and hydroxyapatite. Gelation was induced by adding potassium chloride solution, resulting in a 4 wt% opaque gel. Polymer dispersion was added and shook overnight prior to filtration and washing via centrifugation. The cholesterol and calcium absorbed polymer was obtained by lyophilization. The absorbed cholesterol was extracted by trituration with diethylether and quantified by UV–vis spectroscopy applying the Liebermann–Burchard reagent. The absorbed calcium was quantified by AAS (Figures S87 and S88, Supporting Information).

Cytotoxicity Assay: The native **G2–1** and **G2–2** polymers conjugates were additionally examined in ex vivo cell viability and cell death assays using the renal proximal tubule epithelial cell line RPTEC/TERT1 and the Alamar Blue (or resazurin) and lactate dehydrogenase leakage assays, respectively. Varying concentrations of the polymers were exposed to the cells for 72 h and the fluorescence was measured at 530 nm excitation and 590 nm emission (Figure S89, Supporting Information).

Supporting Information

Supporting Information is available from the Wiley Online Library or from the author.

Acknowledgements

We thank Rose Rosenberg for AUC measurements, Lars Bolk for GPC and DSC measurements, Dr. Markus Drechsler for CryoTEM analysis, Franziska Doll for fluorescence microscopy, and Philipp Secker for cytotoxicity assays and the particle analysis center of the SFB1214 for DLS and zeta-potential measurements. The authors would also like to thank the staff of ESRF (Grenoble, France) for assistance and support in collecting the SAXS data at beamline BM29. C.R.A. and J.A. thank the SFB1214 (A7 and A2) and the authors are grateful about the financial support from the Zukunftskolleg and the University of Konstanz.

Conflict of Interest

A patent is pending for the **G1** generation of polymers described in this paper.

Keywords

block copolymer, nanocomposites, polymer chemistry, scale dissolution, self-assembly

[1] Y. Mai, A. Eisenberg, *Chem. Soc. Rev.* **2012**, *41*, 5969.
[2] S. Darling, *Prog. Polym. Sci.* **2007**, *32*, 1152.
[3] G. Riess, *Prog. Polym. Sci.* **2003**, *28*, 1107.
[4] A. Lavasanifar, J. Samuel, G. S. Kwon, *Adv. Drug Delivery Rev.* **2002**, *54*, 169.
[5] K. Kataoka, A. Harada, Y. Nagasaki, *Adv. Drug Delivery Rev.* **2012**, *64*, 37.
[6] A. Rösler, G. W. Vandermeulen, H.-A. Klok, *Adv. Drug Delivery Rev.* **2012**, *64*, 270.
[7] S. Förster, M. Antonietti, *Adv. Mater.* **1998**, *10*, 195.
[8] H. Cölfen, *Macromol. Rapid Commun.* **2001**, *22*, 219.
[9] M. Jones, J. Leroux, *Eur. J. Pharm. Biopharm.* **1999**, *48*, 101.
[10] X. Duan, J. Xiao, Q. Yin, Z. Zhang, H. Yu, S. Mao, Y. Li, *ACS Nano* **2013**, *7*, 5858.
[11] L. Wei, C. Cai, J. Lin, T. Chen, *Biomaterials* **2009**, *30*, 2606.
[12] R. Cheng, F. Meng, C. Deng, H.-A. Klok, Z. Zhong, *Biomaterials* **2013**, *34*, 3647.
[13] S. Lv, Z. Tang, M. Li, J. Lin, W. Song, H. Liu, Y. Huang, Y. Zhang, X. Chen, *Biomaterials* **2014**, *35*, 6118.
[14] D. Zhang, A. Tamilselvan, *J. Mater. Sci.: Mater. Med.* **2007**, *18*, 79.
[15] L. R. Pratt, D. Chandler, *J. Chem. Phys.* **1977**, *67*, 3683.
[16] L. F. Pacheco, A. M. Carmona-Ribeiro, *J. Colloid Interface Sci.* **2003**, *258*, 146.
[17] S. Kim, Y. Shi, J. Y. Kim, K. Park, J.-X. Cheng, *Expert Opin. Drug Delivery* **2010**, *7*, 49.
[18] L. Bell, H. Mika, B. Kruger, *Arch. Oral Biol.* **1978**, *23*, 329.
[19] M. E. Haberland, J. A. Reynolds, *Proc. Natl. Acad. Sci. USA* **1973**, *70*, 2313.
[20] N. Townsend, L. Wilson, P. Bhatnagar, K. Wickramasinghe, M. Rayner, M. Nichols, *Eur. Heart J.* **2016**, *37*, 3232.
[21] M. di Cagno, *Molecules* **2017**, *22*, 1.
[22] D. Stelzl, T. T. Nielsen, T. Hansen, M. di Cagno, *Int. J. Pharm.* **2015**, *496*, 896.
[23] V. M. Atger, M. de la Llera Moya, G. W. Stoudt, W. V. Rodrigueza, M. C. Phillips, G. H. Rothblat, *J. Clin. Invest.* **1997**, *99*, 773.
[24] L. Kritharides, M. Kus, A. J. Brown, W. Jessup, R. T. Dean, *J. Biol. Chem.* **1996**, *271*, 27450.
[25] S. Zimmer, A. Grebe, S. S. Bakke, N. Bode, B. Halvorsen, T. Ulas, M. Skjelland, D. De Nardo, L. I. Labzin, A. Kerksiek, C. Hempel, M. T. Heneka, V. Hawxhurst, M. L. Fitzgerald, J. Trebicka, I. Björkhem, J.-Å. Gustafsson, M. Westerterp, A. R. Tall, S. D. Wright, T. Espevik, J. L. Schultze, G. Nickenig, D. Lütjohann, E. Latz, *Sci. Transl. Med.* **2016**, *8*, 333ra50.
[26] D. R. Lewis, K. Kamisoglu, A. W. York, P. V. Moghe, *Wiley Interdiscip. Rev.: Nanomed. Nanobiotechnol.* **2011**, *3*, 400.
[27] M. Schiener, M. Hossann, J. R. Viola, A. Ortega-Gomez, C. Weber, K. Lauber, L. H. Lindner, O. Soehnlein, *Trends Mol. Med.* **2014**, *20*, 271.
[28] A. J. Lusis, *Nature* **2000**, *407*, 233.
[29] J. Lu, Y. Zhao, X. Zhou, J. H. He, Y. Yang, C. Jiang, Z. Qi, W. Zhang, J. Liu, *Biomacromolecules* **2017**, *18*, 2286.
[30] C. S. Thaxton, W. L. Daniel, D. A. Giljohann, A. D. Thomas, C. A. Mirkin, *J. Am. Chem. Soc.* **2009**, *131*, 1384.
[31] B. Senthilmurugan, B. Ghosh, S. Sanker, *J. Ind. Eng. Chem.* **2011**, *17*, 415.
[32] A. Verch, D. Gebauer, M. Antonietti, H. Colfen, *Phys. Chem. Chem. Phys.* **2011**, *13*, 16811.
[33] E. Mavredaki, A. Neville, K. Sorbie, *Appl. Surf. Sci.* **2011**, *257*, 4264.
[34] G. H. Nancollas, W. Wu, *J. Cryst. Growth* **2000**, *211*, 137.
[35] A. Peytcheva, M. Antonietti, *Angew. Chem., Int. Ed.* **2001**, *40*, 3380.
[36] G. M. v. Rosmalen, *Chem. Eng. Commun.* **1983**, *20*, 209.
[37] K. S. Krannig, H. Schlaad, *J. Am. Chem. Soc.* **2012**, *134*, 18542.
[38] I. Astafieva, X. F. Zhong, A. Eisenberg, *Macromolecules* **1993**, *26*, 7339.
[39] E. Tomaszewska, K. Soliwoda, K. Kadziola, B. Tkacz-Szczesna, G. Celichowski, M. Cichomski, W. Szmaja, J. Grobelny, *J. Nanomater.* **2013**, *2013*, 60.

[40] L. L. Abell, B. B. Levy, B. B. Brodie, F. E. Kendall, *J. Biol. Chem.* **1952**, *195*, 357.
[41] J. S. Wilkhu, D. Ouyang, M. J. Kirchmeier, D. E. Anderson, Y. Perrie, *Int. J. Pharm.* **2014**, *461*, 331.
[42] S. Sevimli, F. Inci, H. M. Zareie, V. Bulmus, *Biomacromolecules* **2012**, *13*, 3064.
[43] F. R. Maxfield, D. Wüstner, in *Methods in Cell Biology* (Eds: P. Gilbert Di, R. W. Markus), Vol. *108*, Academic Press, New York **2012**, pp. 367–393, Chap. 17.
[44] X. Guo, A. Gutsche, H. Nirschl, *J. Nanopart. Res.* **2013**, *15*, 2058.
[45] T. Yokoi, M. Kawashita, C. Ohtsuki, *J. Asian Ceram. Soc.* **2013**, *1*, 155.
[46] J. Willis, *Spectrochim. Acta* **1960**, *16*, 259.
[47] A. Harada, K. Kataoka, *Macromolecules* **1995**, *28*, 5294.
[48] C. Koppe, M. Rodríguez, K. Winkler, J. Pietzsch, K. Neumann, N. E. Hiemann, R. Hetzer, M. Malmsten, G. Siegel, *Res. Complementary Med.* **2009**, *16*, 237.
[49] P. F. Secker, L. Luks, N. Schlichenmaier, D. R. Dietrich, *ALTEX* **2018**, *35*, 223.